J. Biochem. 125, 916-922 (1999)

Two Concentric Protein Shell Structure with Spikes of Silkworm *Bombyx mori* Cytoplasmic Polyhedrosis Virus Revealed by Small-Angle Neutron Scattering Using the Contrast Variation Method[1]

Masahiro Tomita,* Tomokazu Hasegawa,† Tomitake Tsukihara,† Shigetoshi Miyajima,* Michihiro Nagao,‡ and Mamoru Sato§,2

*Department of Chemistry for Materials, Mie University, 1515 Kamihama, Tsu 514-8507; †Institute for Protein Research, Osaka University, 3-2 Yamada-oka, Suita, Osaka 565-0871; ‡Neutron Scattering Laboratory, Institute for Solid State Physics, The University of Tokyo, 106-1 Shirakata, Tokai, Naka, Ibaraki 319-1106; §Graduate School of Integrated Science, Yokohama City University, 22-2 Seto, Kanazawa-ku, Yokohama 236-0027

Received January 7, 1999; accepted February 5, 1999

The overall and internal structures of the silkworm *Bombyx mori* cytoplasmic polyhedrosis virus was investigated by small-angle neutron scattering using the contrast variation method. Data were collected in aqueous buffer solutions containing 0, 50, 75, and 100% D_2O in the q range of 0.002 to 0.0774 Å^{-1} at 5°C. The radius of gyration at infinite contrast was estimated to be 336 Å. The contrast matching point of the virus was determined to correspond to about 50% D_2O level, evidence that the virus is composed of protein and nucleic acid. The virus was basically spherical and had a diameter of about 700 Å. The main feature of its structure is the clustering of protein into two concentric shells separated by about 100 Å. Most of the RNA moieties are located in the central core and between these two protein shells. However, the distance distribution function $P(r)$ showed a minor distribution beyond a distance of $r=700$ Å, with a maximum particle distance of the virus of 1350 Å. This is indicative of an external structure region with very low scattering density, in addition to the basic spherical structure. This external region is thought to correspond to twelve pyramidal protruding spikes shown by electron microscopic studies.

Key words: contrast variation, cytoplasmic polyhedrosis virus, neutron scattering, small-angle scattering.

Cytoplasmic polyhedrosis viruses (CPV), a family of the *Reoviridae*, are characterized by the formation of large intracytoplasmic occlusion bodies (*1*) and the possession of ten double-stranded RNA (dsRNA) segments as a genome (*2*). The insect occlusion bodies, which have been reported in more than 100 insect species, frequently form in the midgut epithelium after virus infection (*1, 3*) and are considered to be a mode of virion protection during the transfer between host cells. The protein that forms the occlusion bodies is called polyhedrin and is encoded by the viral genome, segment 10. In most cases, the polyhedrin has a molecular weight of between 25,000 and 31,000 (*4, 5*). The occlusion bodies are formed by the crystallization of the viral polyhedrin polypeptide around infectious viral particles.

The shape of the occlusion body is characteristic of the particular virus. Electron microscopic studies have shown that *Bombyx mori* cytoplasmic polyhedrosis virus (BmCPV) is classified into nine strains (I, H, P, A, B, B1, B2, C1, and C2) (*1*). The polyhedrins that form the regular hexahedral (H strain) and regular icosahedral (I strain) polyhedra are both composed of 248 amino acids with a deduced molecular weight of 28,500, and their amino acid sequences differ from each other at four positions (*6, 7*). Lately, nucleotide sequences of segments 8 and 9 of BmCPV strains H and I have been determined (*8, 9*) and its genome analyses are swiftly proceeding.

BmCPV consists of dsRNA and protein, and forms a very large particle of a biological supramolecular complex with a molecular weight of about 10^8. Its inner structure was originally shown by Miura *et al.* (*10, 11*). Further elucidation of the structure-function relationship of the virus particle and the distribution of protein and dsRNA moieties within the particle awaits the analyses of not only the overall structure but also the internal structure of the BmCPV particle in solution. We therefore performed small-angle neutron scattering (SANS) analysis of the BmCPV particle in solution using the contrast variation method.

[1] This work was supported in part by Grants-in-Aid (No. 06276103, No. 09558093, and No. 10179101 to M.S.) for Scientific Research from the Ministry of Education, Science, Sports and Culture of Japan, and was performed with the approval of the Neutron Scattering Program Advisory Committee (Proposal Nos. 95-165, 96-125, and 97-78).

[2] To whom correspondence should be addressed. Mamoru Sato, Graduate School of Integrated Science, Yokohama City University, 22-2 Seto, Kanazawa-ku, Yokohama 236-0027. E-mail: msato@yokohama-cu.ac.jp

Abbreviations: D_{max}, maximum particle distance; Rg, radius of gyration; SANS, small-angle neutron scattering; BmCPV, *Bombyx mori* cytoplasmic polyhedrosis virus.

MATERIALS AND METHODS

Purification and Sample Preparation for SANS Measurement—BmCPV was purified as reported before (*9*), except that occlusion bodies including BmCPV particles were treated in the presence of 0.2 M $NaHCO_3$-Na_2CO_3, pH 10.8, at 4°C for 60 min with gentle agitation, instead of vortexing, in order to recover BmCPV particles as a fully intact form. Two stock solutions were prepared from the purified virus solution with 10 mM Tris-HCl buffer, pH 8, containing 1 mM EDTA with different D_2O/H_2O contents, one containing 100% H_2O and the other 100% D_2O. Each solution was concentrated to 6.5–7.0 mg/ml in a Centricon-30 concentrator (Amicon Division, W.R. Grace & Co., USA), and dialyzed against 10 mM Tris-HCl buffer, pH 8, containing 1 mM EDTA and four levels of D_2O contents: 0, 50, 75, and 100%. These virus solutions were transferred with their corresponding buffer solvents to standard quartz cells of 1 mm path length for the 0% D_2O solution, 2 mm path length for the 50% D_2O solution, and 3 mm path length for the 75 and 100% D_2O solutions. The final virus concentrations of the solutions were determined as described by Lowry *et al.* (*12*) with bovine serum albumin as a standard.

SANS Measurement—The SANS-U instrument, installed at the C1-2 beam port of the JRR-3M reactor of the Japan Atomic Energy Research Institute, Tokai, was used to measure the low-angle neutron scattering intensity as a function of momentum transfer, q ($q=4\pi\sin\theta/\lambda$, 2θ: scattering angle, λ: wavelength of neutron). Details of the data collection method and the design of the equipment have been reported elsewhere (*13*). Neutrons with a wavelength, λ, of 7.0 Å were chosen, with sample-to-detector distances of 4 and 12 m, to cover the q range of 0.002 to 0.0774 $Å^{-1}$. The beam size at the sample position was about 8 mmϕ. A wavelength bandwidth, $\Delta\lambda/\lambda$, of about 10% was obtained with a velocity selector (Dornier, Germany) operated at 16,300 rpm. Scattered neutrons were detected with a helium-filled two-dimensional position-sensitive detector (Ordela, USA). The sample solutions in the quartz cells were placed in an automatic sample changer and maintained in helium gas at 5°C with a Peltier device.

Data Reduction and Analysis—The raw SANS datasets were normalized for a common monitor count and for the same sample cell thickness, and then corrected for transmission. Each data array was divided pixel-by-pixel by means of an isotropic incoherent scattering array measured with H_2O, to correct for differences in the sensitivities of different parts of the detector. A circular average was then made to obtain a one-dimensional intensity profile as a function of q. The intensity profile did not change significantly on desmearing for the effects of beam divergence and wavelength spread; therefore, these corrections were not applied. The data thus treated were finally corrected for the background scattering from the corresponding buffer solution. The SANS datasets collected at different sample-to-detector distances (0, 75, and 100% D_2O datasets) were merged together and then subjected to the structural analysis. The reliability factors for merging the datasets, R_{merge}, were 0.059, 0.042, and 0.029 for 0, 75, and 100% D_2O datasets, respectively. The effect of the particle concentration on the scattering profile was examined using the datasets obtained in 100% D_2O solutions with different virus concentrations.

THEORETICAL BACKGROUND

Contrast Variation Method—In "single particle" scattering, the excess scattering density, $\Delta\rho(\vec{r},\rho_S)$ that gives the neutron scattering from the particle can be formulated as:

$$\Delta\rho(\vec{r},\rho_S)=\Delta\rho(\vec{r},\bar{\rho})+(\bar{\rho}-\rho_S)\cdot v(\vec{r}) \quad (1)$$

where $\vec{r}$ is the real space vector and $\bar{\rho}$ the mean scattering density of the particle. $v(\vec{r})$ gives the shape of the particle, and is defined as unity within the particle and zero elsewhere. ρ_S is the scattering density of the solvent and is constant throughout the solution. $\Delta\rho(\vec{r},\bar{\rho})$ expresses variation in the scattering density to $\bar{\rho}$ within the particle and therefore provides information on the internal structure of the particle.

In a dilute solution, where the interparticle interference effect is neglected to the extent that the "single particle" scattering is approved, the scattering intensity, $I(q)$, from one particle is given by the spherical average of the square of the Fourier transform of $\Delta\rho(\vec{r},\rho_S)$. This is expressed by three basic functions, $I_P(q)$, $I_{PV}(q)$, and $I_V(q)$, called the characteristic functions (*14*):

$$I(q)=I_P(q)-(\bar{\rho}-\rho_S)\cdot I_{PV}(q)+(\bar{\rho}-\rho_S)^2\cdot I_V(q) \quad (2)$$

where $I_V(q)$ is the shape function of the particle obtained from the spherical average of the square of the Fourier transform of $v(\vec{r})$; $I_P(q)$ the scattering intensity from the variation of scattering density within the particle, $\Delta\rho(\vec{r},\bar{\rho})$; and $I_{PV}(q)$ the cross term of $I_P(q)$ and $I_V(q)$. For the very small q range, Eq. 2 can be expanded as to the first two terms as follows:

$$I(q)=v^2\cdot(\bar{\rho}-\rho_S)^2\cdot(1-Rg^2\cdot q^2/3+\cdots\cdots) \quad (3)$$

$$\cong v^2\cdot(\bar{\rho}-\rho_S)^2\cdot\exp(-Rg^2\cdot q^2/3) \quad (4)$$

$$=I(0)\cdot\exp(-Rg^2\cdot q^2/3) \quad (5)$$

where v is $\int v(\vec{r})\mathrm{d}v_r$ and defines the total excluded volume of the particle, and Rg and $I(0)$ the radius of gyration of $\Delta\rho(\vec{r},\rho_S)$ and scattering intensity at $q=0$, respectively. Rg and $I(0)$ can be obtained from the initial slope and $q=0$ intercept of the best-fit straight line of the $\ln I(q)$ *vs.* q^2 plot [the Guinier plot (*15*)], which shows linear relationship for the mono-dispersed solute particles. Rg depends on the contrast, $(\bar{\rho}-\rho_S)$, and is expressed (*14, 16, 17*) as:

$$Rg^2=Rv^2+\alpha\cdot(\bar{\rho}-\rho_S)^{-1}-\beta\cdot(\bar{\rho}-\rho_S)^{-2} \quad (6)$$

where

$$Rv^2=v^{-1}\int r^2\cdot v(\vec{r})\mathrm{d}v_r$$

$$\alpha=v^{-1}\int r^2\cdot\Delta\rho(\vec{r},\bar{\rho})\mathrm{d}v_r$$

$$\beta=v^{-2}\cdot\left|\int\vec{r}\cdot\Delta\rho(\vec{r},\bar{\rho})\mathrm{d}v_r\right|^2$$

Rv is Rg at infinite contrast $[(\bar{\rho}-\rho_S)^{-1}=0]$ and corresponds to the Rg of the particle shape, $v(\vec{r})$. The coefficients, α and β, are values that depend on the distribution of the scattering density within the particle and are informative for the internal structure analysis. By definition, α shows the relative distribution of the high and low scattering density regions within the particle, and β is a function

of the symmetry of the internal structure: that is, $\beta \cdot (\bar{\rho} - \rho_S)^2$ corresponds to the distance between the centers of masses of $\Delta\rho(\vec{r},\rho_S)$ and $v(\vec{r})$.

The Distance Distribution Function—The distance distribution function, $P(r)$ (*18*), is given by the Fourier transform of $I(q)$, as follows:

$$P(r) = \frac{r}{2\pi^2}\int_0^\infty q \cdot I(q) \cdot \sin(q \cdot r) dq \quad (7)$$

The $P(r)$ function multiplied by 4π represents the number of vectors with the distance, r, found in the combination of any small volume element, i, with any other volume element, j. The profile of $P(r)$ is sensitive to both the overall structure (shape) and internal distribution of the scattering density of the particle. The $P(r)$ is a good test of the quality of $I(q)$ data, and is expected to vanish for the distance, r, equal to the maximum particle dimension, D_{max}, which corresponds to the diameter for spherical particle.

The Radial Scattering Density Distribution Function—The radial scattering density distribution function, $\rho(r)$, can be obtained for a particle with spherically symmetric structure in solution by the Fourier transform of the structure factor, $F(q)$, as follows:

$$\rho(r) - \rho_S = \frac{1}{2\pi r}\int_0^\infty q \cdot F(q) \cdot \sin(q \cdot r) dq \quad (8)$$

where $F(q)$ is related to $I(q)$ by $I(q) = |F(q)|^2$. In the absence of instrumental effects, $I(q)$ would vanish at several q values (zero-minima), and give $F(q)$ of alternating sign at each zero-minimum (*19, 20*). However, such zero-minima of $I(q)$ profile can not be observed in experimental practice with macromolecular structures (Fig. 1) because of a minor degree of size heterogeneity, time dependent deformation of the flexible structure, and so on. All these effects smear the experimental $I(q)$ profile and result in the filling up of the zero-minima. The problem of zero-minima was solved by decomposing $I(q)$ into two terms, one ascribed to the spherical average and the other to the deviation from sphericity (*21*).

RESULTS AND DISCUSSION

Small-Angle Neutron Scattering Profile—The effect of the interparticle interference on the SANS profile was first examined by using the datasets for the 100% D_2O solutions with virus concentrations of 1, 3, and 5 mg/ml. The SANS profiles showed no variation of the radius of gyration, *Rg*, estimated from the Guinier plots (data not shown), with these concentrations, indicating that a virus concentration less than 5 mg/ml permitted interparticle interference effects to be safely neglected.

Figure 1 shows the SANS intensity profiles, $I(q)$ of BmCPV obtained in 0, 75, and 100% D_2O with a concentration of 5 mg/ml. All these profiles had a central maximum at $q = 0$ and four subsidiary maxima that reflect the typical behavior of scattering from a spherical particle. In the 50% D_2O dataset, however, scattering intensities from BmCPV solution almost equalled those from the corresponding buffer solution containing 50% D_2O, and resulted in net scattering intensities with very weak and noisy signals (Fig.

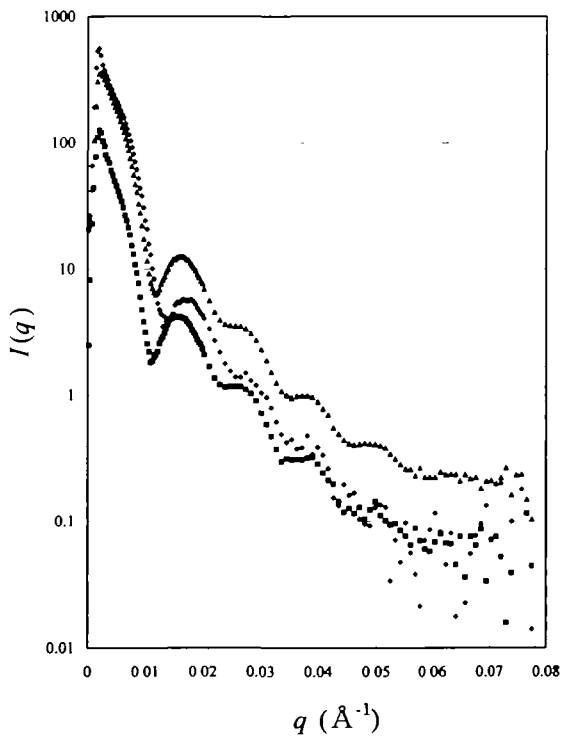

Fig. 1. **SANS intensity profiles, $I(q)$, of BmCPV solutions containing 0% D_2O (◆), 75% D_2O (■), and 100% D_2O (▲).** BmCPV concentration of each solution is 5 mg/ml. Note that the q range less than $q = 0.002$ Å^{-1} was covered by a beam stopper in order to protect the neutron detector.

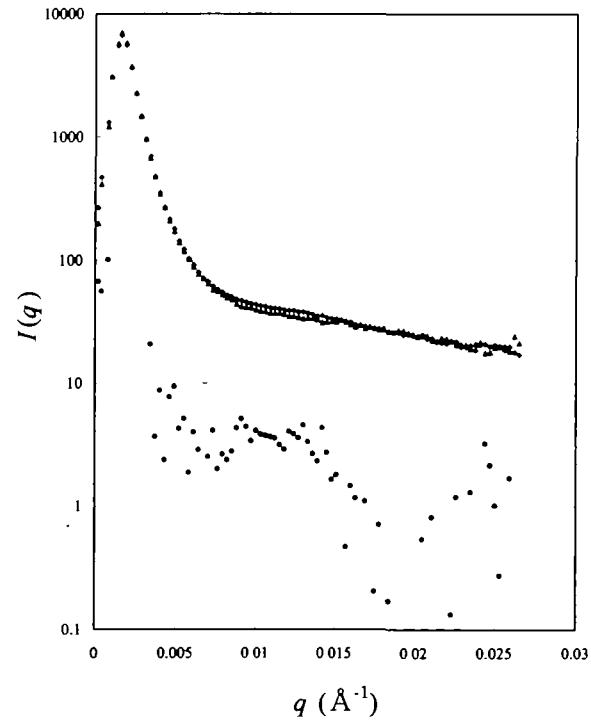

Fig. 2. **SANS intensity profiles of (◆) BmCPV solution containing 50% D_2O, $I(q)_S$, (■) buffer solution containing 50% D_2O, $I(q)_B$ and (●) $I(q)_S - I(q)_B$.** $I(q)_S$ and $I(q)_B$ are intensity datasets just after circular averaging (see text). BmCPV concentration is 5 mg/ml. Note that the q range less than $q = 0.002$ Å^{-1} was covered by a beam stopper in order to protect the neutron detector.

2). This indicates that the mean scattering density, $\bar{\rho}$, of BmCPV particle is close to 50% D_2O level. The SANS profiles of 0, 75, and 100% D_2O datasets were characteristic in that the four subsidiary maxima of 75 and 100% D_2O datasets had almost the same q values but they significantly deviated from those of 0% D_2O dataset. This is strongly indicative of a lack of homogeneity of the scattering density within the particle.

Guinier Plot and Radius of Gyration—Figure 3 shows Guinier plots of the 0, 75, and 100% D_2O datasets, together with best-fit straight lines determined by the least-squares procedure. All the plots showed excellent linearity in the q range of 0.0028 to 0.0043 $Å^{-1}$, indicating that BmCPV is a monodispersed solute particle and free from such secondary effects as the formation of particle aggregates and experimental artifacts in 0, 75, and 100% D_2O. The *Rg*s were estimated to be 317, 373, and 351 Å for 0, 75, and 100% D_2O datasets, respectively. The fact that the *Rg* changed depending on the D_2O content is further indication of a lack of homogeneity of the scattering density within the particle.

Stuhrmann Plot—The fact that the *Rg* changed depending on the D_2O content, that is, the contrast, $(\bar{\rho} - \rho_S)$, means that the BmCPV particle consists of different regions in terms of the scattering density distribution within the particle. We therefore investigated the scattering density distribution within the particle from the analysis of the contrast dependency of *Rg* [Stuhrmann plot (*17*)] according to Eq. 6.

To examine the contrast dependency of *Rg*, we first evaluated the mean scattering density of the particle, $\bar{\rho}$, from Eqs. 4 and 5 as the zero-crossing point (the contrast matching point) with which the square-root of $I(0)$, $\sqrt{I(0)}$, when plotted as a function of the D_2O content gives a best-fit straight line as shown in Fig. 4. The excellent linear relationship of $\sqrt{I(0)}$ with D_2O content is evidence that the BmCPV particle is monodispersed in solution and therefore suitable for SANS analysis using the contrast variation method. From the contrast matching point, the mean scattering density, $\bar{\rho}$, of the particle was estimated to correspond to about 50% D_2O level. This is supported experimentally by the result that SANS intensities from BmCPV solution in 50% D_2O were close to those of the corresponding buffer solution containing 50% D_2O (Fig. 2). The mean scattering density of the particle is reasonable as

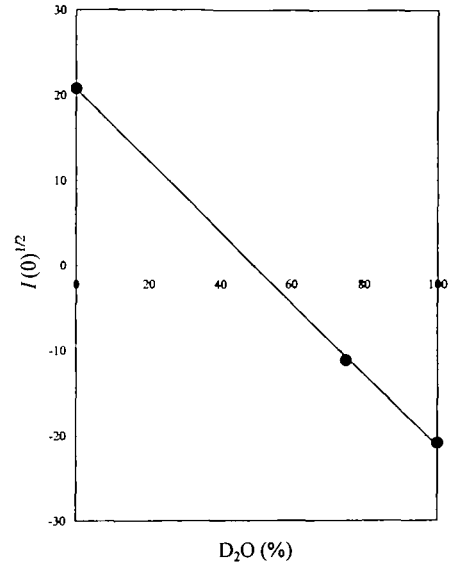

Fig. 4. **Variation of $\sqrt{I(0)}$ with the D_2O content (%) for BmCPV.** $I(0)$ is scattering intensity at $q=0$ and was determined by the least-squares fitting procedure of the Guinier plot. Superimposed is the best-fit straight line determined by the least-squares procedure.

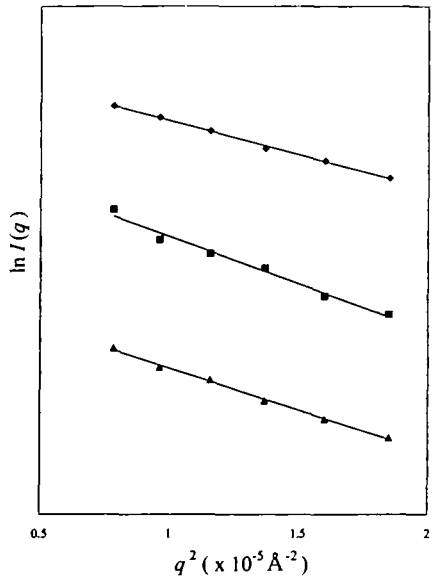

Fig. 3. **Guinier plots of BmCPV solutions containing 0% D_2O (◆), 75% D_2O (■), and 100% D_2O (▲).** BmCPV concentration of each solution is 5 mg/ml. Superimposed are best-fit straight lines, determined by the least-squares procedure, which were used to estimate the values of *Rg* and $I(0)$ (scattering intensity at $q=0$). The ordinates are shifted vertically by an arbitrary amount for clarity.

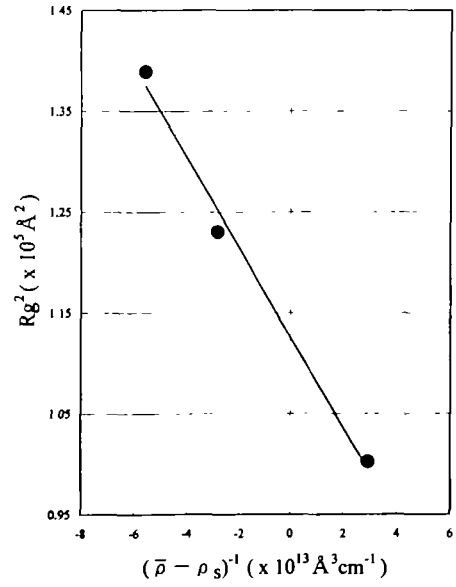

Fig. 5. **Stuhrmann plot of BmCPV.** The data points were best-fittted with a straight line according to the equation, $Rg^2 = Rv^2 + \alpha \cdot (\bar{\rho} - \rho_S)^{-1}$ by the least-squares procedure.

a complex of dsRNA and protein, because the typical scattering densities of RNA and protein moieties correspond to about 70 and 40% D_2O levels, respectively.

The Stuhrmann plot obtained using the $\bar{\rho}$ value of the particle is given in Fig. 5. The almost linear relationship ($\beta=0$ in Eq. 6) indicates that the center of mass of $\Delta\rho(\vec{r}, \rho_S)$ coincides with that of the particle shape, $v(\vec{r})$. Furthermore, the relationship with $\alpha<0$ accounts for the scattering density of the peripheral region of the particle being lower than that of the core region. The *Rg* of the particle shape, *Rv*, was deduced to be 336 Å from the $(\bar{\rho}-\rho_S)^{-1}=0$ intercept of the best-fit straight line superimposed on the Stuhrmann plot. This *Rv* value corresponds to that of a spherical particle with a diameter of 870 Å and homogeneous scattering density [$Rv=a\cdot\sqrt{3/5}$, where $2a$ is a diameter of the spherical particle (*22*)].

The Radial Scattering Density Distribution Function—The Stuhrmann plot indicated that BmCPV is a quasi-spherical particle with radially symmetric distribution of scattering density from the center of mass of the particle. This allows further analysis of the scattering intensity data and has the potential to evaluate the radial distribution of scattering density within the particle using Eq. 8. The sign of $F(q)$ in Eq. 8 was assigned alternately, and that of $F(0)$ was positive for the D_2O content below the contrast matching point of the particle and negative above it. Because of a minor degree of size heterogeneity and time-dependent deformation of the flexible structure and also of deviation from spherical symmetry of scattering density and accuracy of $I(q)$ data, we have used $I(q)$ data up to $q=0.065$ Å^{-1} for 0, 75, and 100% D_2O datasets. This q value corresponds to Bragg spacing, d, of 95 Å, and provides a sufficient amount of $I(q)$ data to calculate the $\rho(r)$ function of the particle.

The $\rho(r)$ functions thus calculated for the various D_2O contents are shown in Fig. 6. These $\rho(r)$ functions were characterized by two peaks, as local maxima, at radii of $r=$ 110 and 225 Å for 0% D_2O and two peaks, as local minima, at radii of $r=150$ and 275 Å for 75 and 100% D_2O. Because the theoretical D_2O levels that correspond to scattering densities of RNA and protein moieties are 68 and 41%, respectively, the $\rho(r)$ function of 75% D_2O strongly reflects the radial distribution of the scattering density of the protein moiety within the particle. Furthermore, the fact that the scattering density of 75% D_2O was higher than $\bar{\rho}$ of the particle means that the protein moiety has negative scattering density and thus gives negative radial distribution. This shows that protein moieties are present mostly at the two peak positions observed as local minima and form a two-concentric-shell structure.

By contrast, the scattering density of 0% D_2O was lower than $\bar{\rho}$ of the particle, and resulted in the two peaks observed as local maxima in the $\rho(r)$ function of 0% D_2O. The profile of the $\rho(r)$ function (0% D_2O) differed from that of 75 or 100% D_2O in terms of the peak positions, and had the two peaks around at radii of $r=110$ and 225 Å. These two peaks were both significantly shifted to shorter radial positions as compared with those of 75 or 100% D_2O. Because the scattering density of 0% D_2O is closer to that of protein than that of RNA, the $\rho(r)$ function of 0% D_2O dominantly reflects the radial scattering density distribution of RNA moiety. The significant shift to the shorter peak positions is accounted for by the presence of dsRNA inside the two concentric shells occupied by protein. These results suggest that protein exists in two concentric shells, one at a radius of $r=150$ Å, the other at a radius of $r=275$ Å, and the latter protein shell occupies the peripheral region of the particle. The remaining core and intermediate regions of the particle are filled up by dsRNA.

The Distance Distribution Function—Although, as shown in Fig. 6, the main radial distributions of the scattering density within the particle disappear beyond a radius of $r=$

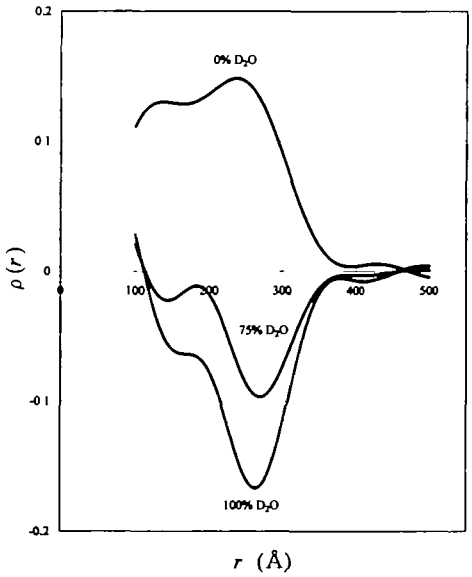

Fig. 6. **Radial scattering density distribution functions of BmCPV in 0, 75, and 100% D_2O contents.** The D_2O contents are indicated near the functions, respectively. The radial scattering density is a relative value and is the difference between that of BmCPV and that of solvent [$\rho(r)-\rho_S$].

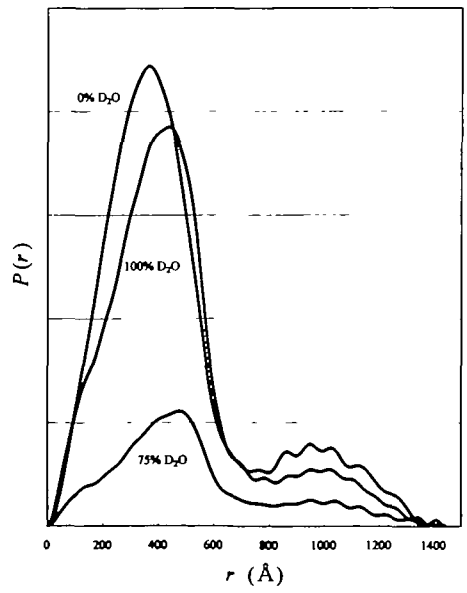

Fig. 7. **Distance distribution functions of BmCPV in 0, 75, and 100% D_2O contents.** The D_2O contents are indicated near the functions.

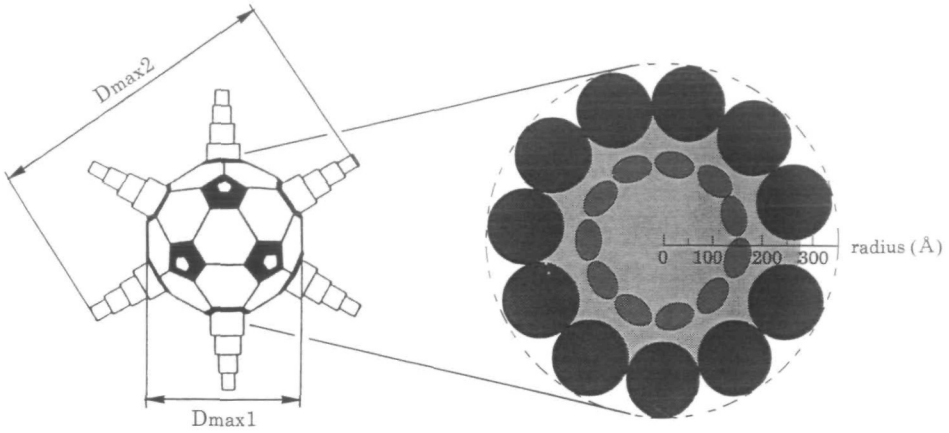

Fig. 8. **Models for the overall structure (left) and the internal structure (right) enlarged from the spherical portion of the overall structure of BmCPV.** The protein molecules in the internal structure are depicted with spheres and ellipsoids, in which the shapes and sizes are shown schematically. Ten segments of dsRNA moieties are present in the core and between the two protein shells. $D_{max}1$ and $D_{max}2$ are maximum dimensions of the spherical portion of the particle and the whole BmCPV particle, respectively. The model for the overall structure (left) was drawn on the basis of that of Ref. *23*.

370 A, small but significant distributions were observed for all D_2O contents. This suggests the presence of a structural region beyond a radius of $r = 370$ Å. In fact, the theoretical Rv value of a spherical particle with a radius of $r = 370$ Å was estimated to be 287 Å from the equation $Rv = r \cdot \sqrt{3/5}$, and was much smaller than the experimental value (Rv = 336 A). To examine this extended structural region, we calculated the distance distribution functions, $P(r)$, for various D_2O contents according to Eq. 7, where $I(q)$ data for $0 \leq q \leq 0.002$ Å^{-1} were extrapolated from the Guinier plot.

Figure 7 shows the $P(r)$ functions calculated from 0, 75, and 100% D_2O datasets. All the profiles of the $P(r)$ functions showed a characteristic feature of minor distributions beyond a distance of $r = 700$ Å, followed by main distributions with different profiles depending on D_2O content. Because the main distance distribution up to the distance of $r = 700$ Å corresponds to the radial distribution up to the radius of $r = 350$ Å in the $\rho(r)$ functions (Fig. 6), the presence of the minor distributions beyond a distance of r = 700 A shows that BmCPV has an external structural region with a very low scattering density outside the spherical surface of the particle. The D_{max} of the whole particle, including the external region, was estimated to be 1350 A, and did not change with the D_2O content.

Structural Model of the BmCPV Particle The structural analysis by the distance distribution functions, $P(r)$ clearly showed the presence of an external region with a very low scattering density. This means that the whole structure of the BmCPV particle is composed of the spherical region with the two concentric protein shell structure and the external region with a very low scattering density. However, such a low scattering density region cannot be assigned as the region for the protein or the RNA moiety, or a mixture of these moieties.

Electron microscopic study has showed that BmCPV is a icosahedral particle with twelve pyramidal protruding spikes (*23, 24*), which is characteristic of CPVs belonging to the *Reoviridae*. This structural characteristic accounts for the presence of the external region with a low scattering density, because the scattering density that corresponds to the spikes is calculated to be very low for small-angle scattering analysis of a dilute solution system because of the spherical average of the square of the Fourier transform of $\Delta\rho(\vec{r}, \rho_s)$, that is, the spherical average of the virus structure. In these points of view, we propose the models for overall and internal structures of BmCPV particle shown in Fig. 8 from the present SANS analysis using the contrast variation method. Our model for overall structure provides 700 and 1350 Å as the maximum dimension for the spherical portion of the particle, $D_{max}1$, and that for the whole particle, $D_{max}2$, respectively, which are both in good agreement with the results obtained from the electron microscopic analysis (*23*).

Because of the limited availability of samples and difficulty in concentrating the virus solution, $I(q)$ datasets of 40-50% D_2O solutions, where the protein components are matched out, revealing only the remaining RNA distribution in the particle, could not be obtained in the present study. In spite of these problems, the present results explain well the overall and internal structures of BmCPV particles, and much can be learned from the architecture of the proposed model. Details of the virus structure will be obtained by the X-ray crystallographic analysis, in which the present results will also be very useful for *ab initio* phasing for the structural solution (*25*) as a starting electron density distribution of the virus, which is in progress.

REFERENCES

1. Hukuhara, T. and Midorikawa, M. (1983) Pathogenesis of cytoplasmic polyhedrosis in the silkworm in *Double-Stranded RNA Viruses* (Compans, R.W. and Bishop, D.H.L., eds.) pp. 405-414, Elsevier Science, New York
2. Fujii-Kawata, I., Miura, K.-I., and Fuke, M. (1970) Segments of genome of viruses containing double stranded ribonucleic acid. *J. Mol. Biol.* **51**, 247 253
3. Payne, C.C. and Mertens, P.P.C. (1983) Cytoplasmic polyhedrosis virus in The *Reoviridae* (Joklik, W.K., ed.) pp. 425 504, Plenum, New York & London
4. Payne, C.C. and Rivers, C.F. (1976) A provisional classification of cytoplasmic polyhedrosis viruses based on the sizes of the RNA genome segments. *J. Gen. Virol.* **33**, 71 85
5. Harrap, K.A. and Payne, C.C. (1979) The structural properties and identification of insect viruses. *Adv. Virus Res.* **25**, 273 355
6. Tomita, M., Kobayashi, J., Mori, A., Hagiwara, K., Nakai, K., Suzuki, Y., and Miyajima, S. (1994) Genetic analysis on morphological differences in the occlusion body of *Bombyx mori* cytoplasmic-polyhedrosis virus. *Protein Eng.* **7**, 1156
7. Miyajima, S., Mori, A., Hagiwara, K., Kobayashi, J., Yoshimura, T., Nakai, K., Suzuki, Y., and Tomita, M. (1998) Microhetero-

geneity in the polyhedrin gene of *Bombyx mori*, a cytoplasmic polyhedrosis virus. *J. Seric. Sci. Jpn.* **67**, 287-294
8. Hagiwara, K., Tomita, M., Kobayashi, J., Miyajima, S., and Yoshimura, T. (1998) Nucleotide sequence of *Bombyx mori* cytoplasmic polyhedrosis virus segment 8. *Biochem. Biophys. Res. Commun.* **247**, 549-553
9. Hagiwara, K., Tomita, M., Nakai, K., Kobayashi, J., Miyajima, S., and Yoshimura, T. (1998) Determination of the nucleotide sequence of *Bombyx mori* cytoplasmic polyhedrosis virus segment 9 and its expression in BmN4 Cells. *J. Virol.* **72**, 5762-5768
10. Miura, K., Fujii-Kawata, I., Iwata, H., and Kawase, S. (1969) Electron-microscopic observation of a cytoplasmic polyhedrosis virus from the silkworm. *J. Invertebr. Pathol.* **14**, 262-265
11. Yazaki, K. and Miura, K. (1980) Relation of the structure of cytoplasmic polyhedrosis virus and the synthesis of its messenger RNA. *Virology* **105**, 467-479
12. Lowry, O.H., Rosebrough, N.J., Farr, A.L., and Randall, R.J. (1951) Protein measurement with the Folin phenol reagent. *J. Biol. Chem.* **193**, 265-275
13. Ito, Y., Imai, M., and Takahashi, S. (1995) Small-angle neutron scattering instrument of the Institute for Solid State Physics, University of Tokyo (SANS-U). *Physica B*, **213** and **214**, 889-891
14. Stuhrmann, H.B. (1982) Contrast variation in *Small Angle X-ray Scattering* (Glatter, O. and Kratky, O., eds.) pp. 197-213, Academic Press, London
15. Guinier, A. and Fournet, G. (eds.) (1955) *Small Angle Scattering of X-Rays*, p. 126, John Wiley and Sons, New York
16. Luzzati, V. and Tardieu, A. (1980) Recent developments in solution X-ray scattering. *Annu. Rev. Biophys. Bioeng.* **9**, 1-29
17. Stuhrmann, H.B. and Miller, A. (1978) Small-angle scattering of biological structures. *J. Appl. Cryst.* **11**, 325-345
18. Pilz, I., Glatter, O., and Kratky, O. (1979) Small-angle X-ray scattering. *Methods Enzymol.* **61**, 148-249
19. Laggner, P. (1982) Lipoproteins and membranes in *Small Angle X-Ray Scattering* (Glatter, O. and Kratky, O., eds.) pp. 336-337, Academic Press, London
20. Chauvin, C., Witz, J., and Jacrot, B. (1978) Structure of the tomato bushy stunt virus: a model for protein-RNA interaction. *J. Mol. Biol.* **124**, 641-651
21. Laggner, P. (1982) Lipoproteins and membranes in *Small Angle X-Ray Scattering* (Glatter, O. and Kratky, O., eds.) p. 335, Academic Press, London
22. Hiragi, Y. and Ihara, S. (1981) Radii of gyration and scattering curves of hollow bodies of homogeneous electron density. *Acta Cryst.* **A37**, 378-382
23. Hosaka, Y. and Aizawa, K. (1964) The fine structure of the cytoplasmic polyhedrosis virus of the silkworm, *Bombyx mori* (Linnaeus). *J. Insect Pathol.* **6**, 53-77
24. Asai, I., Kawamoto, F., and Kawase, S. (1972) On the structure of the cytoplasmic-polyhedrosis virus of the silkworm, *Bombyx mori*. *J. Invertebr. Pathol.* **19**, 279-280
25. Naitow, H., Morimoto, Y., Mizuno, H., Kano, H., Omura, T., Koizumi, M., and Tsukihara, T. (1999) *Ab initio* phase determination for a spherical virus: breaking the centric nature of the initial phases of a spherical-shell model. *Acta Cryst.* **D55**, 77-84